Dynamic Interference Avoidance in the Joint Space-Time Domain with Arbitrary Antenna Formations

Hatef Nouri*, Sanaz Naderi*, Dimitris A. Pados*, George Sklivanitis*, Elizabeth Serena Bentley[†], and Michael J. Medley[†]

*Center for Connected Autonomy and AI, Florida Atlantic University, Boca Raton, FL 33431 USA E-mail: {hnouri, snaderi2021, dpados, gsklivanitis}@fau.edu

†Air Force Research Laboratory, Rome, NY 13440 USA
E-mail: {elizabeth.bentley.3, michael.medley}@us.af.mil

Abstract-We design, implement, and demonstrate a hardware-reconfigurable multiple-input multiple-output (MIMO) transceiver that computes in real-time the transmit multi-antenna beam weight vector and time-domain coded waveform that maximize the signal-to-interference-plus-noise ratio (SINR) at the output of the maximum SINR joint space-time receiver filter. To the best of our knowledge, this is the first demonstration of autonomous hands-free high-throughput communications by jointly optimizing the space and time domain shape of waveforms in heavily congested or contested spectrum environments. Implementation of the self-optimized interference-avoiding MIMO wireless link is carried out on a Radio-Frequency System-on-Chip (RFSoC) software-defined radio (SDR) using the Xilinx Zynq Ultrascale+ RFSoC ZCU111 platform. We experimentally evaluate the performance of the proposed dynamic waveform in a 4x4 MIMO wireless link in terms of pre-detection SINR in the presence of different levels of co-channel interference and arbitrary antenna formations in an indoor laboratory environment.

I. Introduction

Dramatic growth in the capability and use of wireless technologies has supercharged many sectors of society including commerce, transportation, health, science, and defense. However, the proliferation of new applications and infrastructure technologies - such as autonomous navigation and transportation, the Internet-of-Things (IoT), machine-to-machine communications, radar-based geo-sciences, connected AI robotics, next-generation mobile wireless - has created high demand on the electromagnetic spectrum relied on by all types of wireless technologies [1], [2]. Spatially and spectrally neighboring systems change frequently, leading to frequent changes in the characteristics of incoming unwanted energy and the interference impact of outgoing energy [3]. There is a plethora of works on dynamic spectrum access (DSA) and cognitive radio, spanning two decades of research [4]-[7] to improve spectrum utilization by allowing secondary unlicensed users to take advantage of ephemeral transmission opportunities in

This work was supported in part by the National Science Foundation under Grants CNS-2027138, CNS-2117822 and EEC-2133516 and the Air Force Research Laboratory under Grant FA8750-21-1-0500. Distribution A. Approved for public release: Distribution Unlimited: AFRL-2024-3203 on 13 Jun 2024.

space, time, or frequency. We consider spectrum-dependent systems that autonomously adapt and repeatedly optimize, on-the-fly, waveforms at different points in space and time over the continuum of the accessible frequency spectrum. This is key to fully exploit every potential opportunity for reliable communications [8], [9].

Multiple-input multiple-output (MIMO) communication architectures play a key role to unlocking new spectrum [10]. In addition to the vast benefits of MIMO technology including higher channel capacity and reliability, MIMO introduces degrees of freedom in both space and time domains. An array of antenna elements can be used to "shape" a received or transmitted signal, by shifting received signals to coherently combine at a single point. This then can improve the SNR of a received signal, and/or be used to mitigate interference. Directional transmission/reception and space-time precoding/filtering can provide flexibility in waveform shaping for spectrum sharing [11]. A directional space-time waveform design for MIMO interference-avoiding communications is presented in [12], in which the code sequence and angle-ofarrival (AoA) of the received signal are jointly optimized to maximize pre-detection SINR. In [13], a precoder is designed to jointly suppress multi-user interference and multi-cell interference. In [14], multi-antennas at the secondary transmitter are exploited to effectively balance between spatial multiplexing for the cognitive radio transmission and interference avoidance at the primary (spectrum incumbent) receivers. This trade-off is studied from an information-theoretic perspective by characterizing the cognitive user's channel capacity under both its own transmit-power constraint as well as a set of interference-power constraints each imposed at one of the primary receivers. In [15] a distributed deep learning model is proposed for interference avoidance in 5G-enabled IoT. In [16], we investigated the problem of dynamically optimizing MIMO transmit waveforms in a given potentially heavily utilized fixed frequency band with applications in near-field or far-field autonomous machine-to-machine communications. We formally derived two novel model-based machine learning solutions to find the transmitter beam weight vector and the pulse code sequence that maximize the SINR at the output of the maximum SINR joint space-time receiver filter.

In this work, we implement in software-defined radio hardware and experimentally evaluate MIMO transmit waveforms proposed in [16]. To the best of our knowledge, this is first demonstration of a high-throughput MIMO communications link that autonomously optimizes the shape and directionality of the transmit waveform to avoid locally-sensed interference and maximize the SINR at the output of the maximum SINR joint space-time receiver filter. We design and implement the proposed wireless data link on the Xilinx Zynq UltraScale+ RFSoC ZCU111 evaluation kit paired with a custom designed RF frontend. We leverage a combination of software tools including MathWorks Simulink and Xilinx Vivado to target an RFSoC SDR platform and demonstrate dynamic interference avoidance by the adaptive joint space-time waveform shaping MIMO system. We implement (PHY)-layer baseband signal processing functions including the optimization of the MIMO transmit waveform algorithm on the programmable logic (PL) of the RFSoC to enable efficient handling of high-bandwidth data streams with deterministic latency and on-the-fly waveform adaptation. The ARM-based processing system (PS) of the RFSoC organizes the I/O, manages the control signals, and monitors link adaptation parameters. We experimentally evaluate the performance of our 4x4 MIMO wireless link in the presence of co-channel interference generated by the same RFSoC SDR in an indoor laboratory environment. We consider three different transmit power levels for the interferer and demonstrate that the proposed MIMO wireless link can recover under the most adverse conditions and achieve up to 25 dB improvement in pre-detection SINR.

The rest of the paper is organized as follows. Section II, presents the MIMO signal model. Section III discusses the testbed design and implementation details. In Section IV, we discuss experimental results. Section V concludes the paper.

II. MIMO SYSTEM MODEL

We consider a MIMO signal system model with M_t transmit and M_r receive antennas operating over a frequency-flat Rayleigh fading channel. We denote the transmitted signal from the $m_t{}^{th}$ antenna as $x_{m_t}(t)$, $m=1,2,...,M_t$ and the received signal by the $m_r{}^{th}$ antenna $y_{m_r}(t)$, $m_r=1,2,...,M_r$. Without loss of generality, we consider quadrature-phase-shift keying (QPSK) modulation. The transmitter sends information symbol sequence b[n], n=0,1,...,N, at rate 1/T across all antennas on a carrier frequency f_c using an underlying digitally shaped pulse s(t) of duration T. Let us denote the average signal transmitted energy per symbol per antenna by E_T . We consider transmission of the same signal over each transmit antenna, multiplied by a complex beam weight parameter $w_{m_t} \in \mathbb{C}$. Specifically, the signal transmitted from the $m_t{}^{th}$ transmit antenna is given by

$$x_{m_t}(t) = \sqrt{E_T} \sum_{n=0}^{N-1} b[n] s(t - nT) e^{j2\pi f_c t} w_{m_t}, \qquad (1)$$

where $w_{m_t} \in \mathbb{C}$ is the antenna beam weight parameter and $m_t = 1, 2, \ldots, M_t$. The time-domain coded pulse s(t) is given by where $s[l] \in \left\{ \pm 1/\sqrt{L} \right\}$ is the l^{th} chip of the code vector s, and $p_{T_c}\left(\cdot\right)$ is a square-root-raised-cosine (SRRC) pulse with roll-off factor α and duration $T_c = T/L$, and the bandwidth of the transmitted signal is $\beta = (1+\alpha)/T_c$. For clarity in presentation, it is assumed that the individual pulses are normalized to unit energy, i.e., $\int_0^{T_c} \left| p_{T_c}\left(t\right) \right|^2 dt = 1$.

At the receiver side, after carrier frequency downconversion, the receive antennas capture

$$\mathbf{r}_{M_r \times 1}(t) = \sqrt{E_T} \sum_{n=0}^{N-1} b[n] s(t - nT_s) \mathbf{H}^T \mathbf{w}_{M_t} + \mathbf{i}(t) + \mathbf{n}(t)$$
 (2)

where $\mathbf{H} \in \mathbb{C}^{M_t \times M_r}$ denotes the MIMO channel matrix assumed to remain constant over NT_b sec, $\mathbf{w}_{M_t} = \begin{bmatrix} w_1, w_2, \dots, w_{M_t} \end{bmatrix}^T \in \mathbb{C}^{M_t}$ is the transmitter beam weight vector, $\mathbf{n}(t) \in \mathbb{C}^{M_r}$ denotes a complex Gaussian noise process that is assumed white both in time and space, and $\mathbf{i}(t) \in \mathbb{C}^{M_r}$ models comprehensively environmental disturbance of any other form that is sensed locally at the receiver.

Upon pulse matched-filtering and sampling over L pulses at each receive antenna element, the collected values are organized in the form of a space-time data matrix $\mathbf{Y}_{M_r \times L}[n]$. The data matrix is then vectorized to

$$\mathbf{y}_{M_rL\times 1}[n] = Vec\{\mathbf{Y}_{M_r\times L}[n]\} =$$

$$= \sqrt{E_T}b[n](\mathbf{s} \otimes \mathbf{H}^T)\mathbf{w}_{M_t} + \mathbf{i}[n] + \mathbf{n}[n]$$
(3)

where $\mathbf{i}[n]$ and $\mathbf{n}[n]$ denote pulse-matched-filtering interference and white noise in the space-time receiver domain. The "space-time disturbance autocorrelation" matrix is given by

$$\mathbf{R}_{i+n} \triangleq E\left\{ \left(\mathbf{i}[n] + \mathbf{n}[n]\right) \left(\mathbf{i}[n] + \mathbf{n}[n]\right)^{H} \right\} \in \mathbb{C}^{M_r L \times M_r L}. \quad (4)$$

For the rest of the paper, we proceed with the joint-space time waveform optimization algorithm proposed in [16], which takes as input the estimated MIMO channel matrix $\hat{\mathbf{H}} \in \mathbb{C}^{M_t \times M_r}$ and pulse-filtered interference-plus-noise received samples and outputs the jointly optimal transmit beam weight vector $\mathbf{w}_{M_t}^{opt}$ and pulse code sequence \mathbf{s}^{opt} .

III. TESTBED DESIGN AND IMPLEMENTATION

In this section, we describe the design and implementation details of the proposed autonomous MIMO interferenceavoiding wireless link on the RFSoC platform.

A. Software-defined Radio Platform

Our SDR platform is built on the Xilinx Zynq Ultra-Scale+ RFSoC ZCU111 evaluation kit, which is based on the XCZU28DR-2FFVG1517E RFSoC Gen1 chip. The kit is paired with the XM500 RFMC balun transformer add-on card and commercial-off-the-shelf (COTS) amplifiers (Nooelec Vega Barebones - ultra low-noise variable gain amplifier), filters (BLK-89-S+ DC block and VBFZ-925-S+) and VERT900 monopole antennas that are omnidirectional in azimuth with an estimated gain of 3 dBi at 900 MHz. The XM500 add-on card

features 4 Digital-to-Analog-Converters (DACs)/4 Analog-to-Digital-Converters (ADCs) routed to high-frequency and low-frequency baluns and 4 DACs/4 ADCs routed to SMAs for use with external custom baluns and filters. The PL and the ARM PS give us the opportunity to examine hardware-software codesign tradeoffs. We use MathWorks Simulink and Xilinx Vivado to target the RFSoC PL and PS. We leverage the high level of parallelism in FPGAs to implement all the baseband processing of our interference-avoiding MIMO transceiver as a non-feedback pipelined architecture on the PL fabric.

B. Transmitter Design and Frame Structure

The data frame structure is described below. A preamble comprising of pilot/training symbols that are a priori known at the receiver precedes the PHY-layer dataframe. The size of the preamble is pre-set to 128 bytes and remains constant across transmitted frames. Each PHY data frame is divided into 8 subframes. Each subframe consists of M_t MIMO training sequences, pilot sequence, header, payload, and cyclic redundancy check (CRC) data. The 32 bytes training sequences are allocated for a specific transmit antenna and are known a priori to the receiver and are used to estimate the magnitude and phase of the channel to build the estimated MIMO channel matrix. A 128 bytes pilot sequence is transmitted from all transmit antennas with corresponding weights $w_{m_t}, m_t =$ $1, 2, \dots, M_t$, and used for bit-error-rate (BER), error vector magnitude (EVM), and SINR calculations). A 4 byte PHY header contains information about the size of the payload and number of subframes. Each subframe includes a payload of 120 bytes. A CRC of 4 bytes is calculated for each payload and appended at the end of each subframe. Therefore, each subframe is 384 bytes long and a PHY dataframe is 3072 bytes. The transmitter remains idle for the time duration of 1552 bytes after transmission of a frame. This is done purposefully to allow the receiver to collect measurements corresponding to local disturbance (i.e., interference and noise).

The preamble is used to determine the accurate starting point of the data frame. A finite-impulse-response (FIR) filter implements a sliding correlation of the received data stream with the expected reference sequence in the preamble structure. We utilize complementary Golay sequences (CGS) in the packet preamble due to their superior aperiodic autocorrelation characteristics in low SINR and multipath environments [17]. Binary Golay pairs are constant amplitude with no information encoded in their phases. Thus, we can use their reversed complex conjugate signum as coefficients of the FIR filter to facilitate hardware-intensive complex multiplications. At the output of the correlator, the absolute value of the peakto-average ratio is computed and is used as the detection metric to compare to a user-defined tunable threshold. When the magnitude of the sliding correlator exceeds the threshold, a flag is asserted to indicate the presence of the preamble. We utilize the frame detector output to delimit the PHY dataframe and pilot symbols contained therein by asserting the corresponding flags.

At the transmitter, a controller block which is a finite state Moore machine controls packetization with logical signaling. Subsequently, subframe generation generates payload data bits, header, CRC, and appends training sequences. The symbol mapping block is a rectangular QPSK modulator that maps the incoming bits to complex symbols using a gray mapping scheme. The MIMO arrangement block then, takes care of transmitting the training sequence for each transmit antenna in a time-division fashion. In this way, receiver antennas at a given time slot receive the signal transmitted from one Tx antenna and estimate the channel coefficients corresponding to each transmit antenna. The MIMO data block organizes the symbols and creates four identical steams of data for a 4x4 MIMO system. Given code sequence vector $\mathbf{s} \in \{\pm 1/\sqrt{L}\}^L$, the spreading block modulates each QPSK symbol into L=4chips. The packetization block appends preamble to the beginning of each frame and by having a gain coefficient as input adjusts the amplitude of the signal and controls the transmitted energy E_T . The transmit SRRC pulse shaping filter is a finite impulse response (FIR) interpolation filter that upsamples and shapes the incoming chips with 8 samples per chip and an SRRC impulse response. The directionality of the waveform is controlled by the block that multiplies the pulse-shaped waveform with a complex-valued beam weight parameter w_{m_t} at each transmit antenna $m_t = 1, 2, \dots, M_t$. Generated samples with a valid flag are delivered to the corresponding RFSoC's DAC channels for transmission. As a result, the samples generated by each antenna overlap except for the samples corresponding to the training sequences.

C. Receiver Design

The over-the-air transmitted signal is captured using 4 ADC channels with sampling rate of 3.9321 GSps per channel and decimated by a factor of 8. Four parallel channels of 491.52 MSps data are streamed to the FPGA with 4 samples per clock. We further decimate by a factor of 4 to get 4 parallel streams of 1 sample per 122.88 MHz FPGA clock cycle. We consider a frequency-flat Rayleigh fading channel with additive-white-Gaussian noise (AWGN) and the channel coefficients remain constant over the duration of a frame. The received signal is first pulse-matched filtered and then a flag is asserted at the beginning of the frame when the magnitude of the sliding correlator with the CGS preamble exceeds a user-defined threshold.

1) Timing Acquisition and Synchronization: Chip-level timing acquisition is carried out after frame detection and after we downsample the signal by a factor of 8 and move from sample rate of 122.88 MSps to chip rate of $R_c=15.36$ Mchips/sec. Since the output of the frame detection does not provide us with a chip-level accurate estimate of the beginning of the frame, we calculate the sample offset to acquire our chipspaced samples as $\hat{k} = \arg\max_{k=0:7} \frac{1}{P} \sum_{p=0}^{P-1} |r \left(pT_c + kT_s \right)|^2$. We create 8 delayed versions of the received chip-space sequences. Then, we calculate the energy of each sequence and apply a moving average over P=1024 samples for each

sequence. The sequence with the maximum energy indicates the best sampling point.

2) Frequency Synchronization: Due to the mismatch of the transmitter and receiver oscillators, a carrier frequency offset (CFO) will rotate the received signal with an angular speed Δf . The receiver estimates the CFO using the correlation-and-accumulation method [18]. Let P_t denote the number of symbols for one period of the training sequence t[k]. Then, the transmitted training chips have the property $t[k] = t[k+P_tL]$ for $k=0,1,...,P_tL-1$. Using this property, for the duration of received training chips we have $y[k+P_tL] \approx e^{j2\pi\Delta f P_tLT_c}y[k]$. Using linear least squares, and assuming two identical training sequences of total length

 $2P_tL$, CFO can be estimated as $\widehat{\Delta f} = \frac{\sum\limits_{k=0}^{P_tL-1}y[k+P_tL]y^*[k]}{2\pi T_c P_tL}$. The phase at the numerator is efficiently computed using the Coordinate Rotation Digital Computer (CoRDiC) algorithm. The estimated $\widehat{\Delta f}$ value is properly scaled to calculate a phase increment that is fed to a numerically controlled oscillator (NCO) to generate a complex exponential signal at the negative of the offset frequency. The input signal is multiplied by $e^{-j2\pi\widehat{\Delta f}kT_c}$ to compensate CFO.

3) Channel Estimation and Space-Time Matched Filtering: To maximize the pre-detection SINR of the received signal we first pulse match filter the received signal using the SRRC filter and then apply the space-time matched filter $\mathbf{g} = \mathbf{s} \otimes \left(\mathbf{H}^T\mathbf{w}\right) \in \mathbb{C}^{NL \times 1}$, which requires an estimate of the MIMO channel matrix \mathbf{H} . We consider a chip-spaced block flat-fading model with Rayleigh distributed magnitude and uniformly distributed phase. Considering the time slot that the training sequence from the first transmit antenna is transmitted, the channel coefficient between the first transmit and receive

the channel coefficient between the first transmit and receive antenna
$$h_{1,1}$$
 is given by $\hat{h}_{1,1} = \frac{1}{w_1} \sum_{k=0}^{p_1 L-1} y_1[k]t_1^*[P_tL-k]$, where

 w_1 is the beam weight of the first transmit antenna, $y_1[k]$ is the received sequence at the first receive antenna, and $t_1[k]$ is the training sequence from the first transmit antenna. Accordingly, we estimate the remaining coefficients of the MIMO channel matrix $\hat{\mathbf{H}}$ and the space-time filter is designed. After space-time filtering the vectorized received data, despreading operation is carried out followed by subsequent QPSK symbol demapping and bit decoding.

4) Experimental Evaluation Metrics: We calculate the number of flipped bits using the a priori known pilot sequences at the receiver and compare them with the recovered symbols using XOR. The accumulated number of erroneous bits is kept in a register and a counter counts the total number of received bits. The BER is calculated in real-time up until the counter hits 100,000,000 and resets. We calculate average BER using a sliding moving average over 1,000 BER values. The instantaneous EVM and SINR values are measured per subframe by having the reference constellation of QPSK and calculating the distance of the received symbol to the reference point. These values are accumulated and averaged over K data points. The SINR can be found using SINR $\approx 1/(\text{EVM})^2$.

The recovered symbols are streamed out of the FPGA to a host computer using the AXI4 stream interface.

D. Optimization of Waveform Shaping and Directionality

Based on the joint space-time optimization algorithm proposed in [16], we first calculate (estimate) the space-time disturbance autocorrelation matrix $\hat{\mathbf{R}}_{i+n}$. During the idle periods of the transmitter, a flag is asserted at the receiver after sensing the absence of a frame. Considering an idle window of $T_{idle} = N_{idle}T_c$, $M_t = M_r = 4$ and L = 4, we vectorize the received sequence and construct the $\tilde{\mathbf{i}}_{16\times 1}$ locally-sensed disturbance vector. By accumulating and averaging over N_{idle}/L vectors

we get
$$\widehat{\mathbf{R}}_{i+n} = \frac{L}{N_{idle}} \sum_{k=0}^{N_{idle}/L-1} \left(\widetilde{\mathbf{i}}_{16\times 1}[k]\right) \left(\widetilde{\mathbf{i}}_{16\times 1}[k]\right)^{H}$$
. Im-

plementing $\widehat{\mathbf{R}}_{i+n}^{-1}$, calculating the maximum-eigenvalue eigenvector $\widehat{\mathbf{q}}_{\max}$ and solving the joint space-time waveform optimization problem in [16] is computationally expensive for the PL. Considering that the space-time disturbance autocorrelation matrix changes slowly or it is relatively constant over the duration of a few frames, and the channel coherence time is large enough, we distribute the workload of optimization to the PS based on our HW/SW co-design. For this reason, the 256 components of the $\widehat{\mathbf{R}}_{i+n}$ matrix, and 16 components of the $\widehat{\mathbf{H}}$ matrix are streamed to the processor using the AXI4 lite interface. On the processor side, $\widehat{\mathbf{R}}_{i+n}^{-1}$ and $\widehat{\mathbf{q}}_{\max}$ are calculated. Already having $\widehat{\mathbf{H}}$, we follow the steps described in Algorithm 2 in [16] to determine the optimum values for waveform shaping \mathbf{s}^{opt} and directionality $\mathbf{w}_{M_t}^{opt}$ which are then fed back to the Tx for interference avoidance.

Algorithm 2 of [16]: Joint space-time waveform optimization

Input: Pulse-filtered interference-plus-noise received samples; estimated channel matrix $\mathbf{H} \in \mathbb{C}^{M_t \times M_r}$.

- 1: Calculate (estimate) space-time disturbance autocorrelation matrix $\mathbf{R}_{i+n} \in \mathbb{C}^{M_rL \times M_rL}$.
- 2: Calculate minimum-eigenvalue eigenvector of \mathbf{R}_{i+n} , $\mathbf{q}_{s-t} \in \mathbb{C}^{M_rL}$.
- 3: Find optimum code $\mathbf{s}^{opt} \in \{\pm 1/\sqrt{L}\}^L$ (or other alphabet) by discrete search over $||\{\mathbf{I} (\mathbf{s} \otimes \mathbf{H}^T) | (\mathbf{s}^T \otimes \mathbf{H}^*)(\mathbf{s} \otimes \mathbf{H}^T)]^{-1}(\mathbf{s}^T \otimes \mathbf{H}^*)\}\mathbf{q}_{s-t}||^2$.
- 4: Find jointly optimal beam weight vector $\mathbf{w}_{M_t}^{opt}$ by inserting \mathbf{s}^{opt} in $\mathbf{w}_{M_t}^{opt} = inv[(\mathbf{s}^T \otimes \mathbf{H}^*)(\mathbf{s} \otimes \mathbf{H}^T)](\mathbf{s}^T \otimes \mathbf{H}^*)\mathbf{q}_{s-t}$. Output: $\mathbf{w}_{M_t}^{opt}$, \mathbf{s}^{opt} .

Fig. 1: Joint space-time waveform optimization algorithm [16].

IV. EXPERIMENTAL RESULTS

We experimentally evaluate the performance of the joint space-time waveform optimization algorithm proposed in [16] for high-throughput resilient MIMO communication in the presence of co-channel interference and arbitrary antenna formations in an RFSoC-based testbed in an indoor laboratory environment. An RFSoC SDR is utilized to control the transmitter and receiver of the MIMO link and the co-channel

interferer; all controlled by a custom MATLAB app that is running on a host PC. We test both linear and square antenna formations considering a carrier frequency of $f_c = 900$ MHz. We place the Rx antennas 2 m away from the Tx and interferer antennas. To assess the performance of our MIMO link, we consider two operation modes: 1) static channelization using an arbitrarily selected fixed (non-optimized) space-time waveform; 2) adaptive channelization with real-time optimized waveform shape and directionality according to [16]. Under normal operation (i.e., when the interferer is turned off), both static and adaptive channelization systems exhibit similar predetection SINR performance. However, only the adaptive system can adapt its waveform to avoid the in-band interference and restore the SINR performance of the disrupted link. We test binary antipodal codes of length L=4 for shaping the time-domain coded pulse-shaped waveforms and we vary the number of samples per chip U. The excess bandwidth parameter of the SRRC is set to $\alpha = 0.5$ which leads to bandwidth occupancy of $11.5 \,\mathrm{MHz}$ with $U = 16, \,23 \,\mathrm{MHz}$ with U=8, and $46\,\mathrm{MHz}$ with U=4. We consider a cochannel interferer that is using the same modulation (QPSK), an arbitrarily selected code and transmits continuously at the same carrier frequency and same bandwidth with the MIMO link to effectively disrupt its performance. The adaptive channelization subsystem at the receiver calculates an estimate of the disturbance autocorrelation matrix \mathbf{R}_{i+n} by sample averaging signal-absent received signal snapshots over 2048 chips that are acquired during the Tx's idle periods.

Figure 2, depicts the post-filtering SINR estimated at the receiver of the 11.5 MHz system under static and adaptive channelization. Each data point in the plot is the result of averaging the pre-detection SINR over 128 consecutive frames. Initially, the system exchanges around 25,000 frames using a fixed (non-optimized) arbitrary waveform. Next, the interferer turns on using the same time-domain coded waveform and almost 25,000 more frames are transmitted. Finally, with the interferer still on, adaptive channelization is enabled manually to autonomously optimize the waveform and 25,000 frames are transferred using the max-SINR optimal space-time waveform. We note that arbitrarily selected waveforms will have a more favorable interaction with certain interferer profiles than others, and head-to-head comparison of SINR curves can be misleading. Nevertheless, varying the transmit power of the interferer helps us better understand the impact of the proposed MIMO waveform optimization method in real-world spectrum congested environments. We consider three different transmit power settings for the interferers. Specifically, with respect to the power of the signal of interest, we consider $P_{S/I} = 4$, 2, and 0 dB. We observe that the average SINR decreases 16.5, 28, and 33 dB respectively. As the co-channel interferer occupies the same-band and carrier with the link of interest, it significantly degrades the link performance. The proposed adaptive MIMO optimized waveform demonstrates an improvement of 11, 26, and 27 dB in pre-detection SINR.

Figure 3, shows the pre-detection SINR estimated at the receiver of the 23 MHz system under static and adaptive

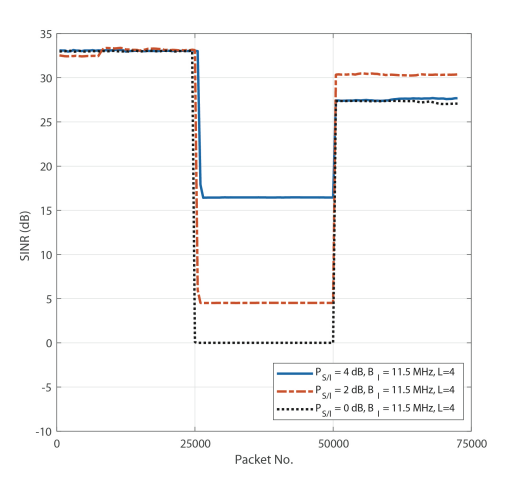


Fig. 2: Pre-detection SINR vs. packet no. in the presence of a co-channel same-band interferer ($\beta = 11.5$ MHz).

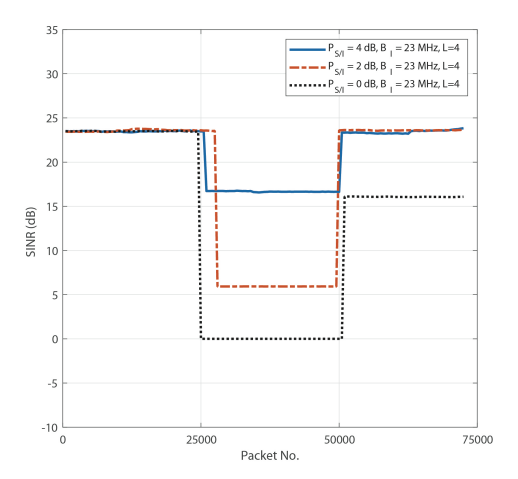


Fig. 3: Pre-detection SINR vs. packet no. in the presence of a co-channel same-band interferer ($\beta = 23$ MHz).

channelization. For the 23 MHz system, the average SINR decreases by 6.8, 17.5, and 23.5 dB for $P_{S/I} = 4$, 2, and 0 dB, respectively. The adaptive system offers a significant improvement of 6.6, 17.7, and 16 dB compared to the static (non-optimized waveform) system in the presence of cochannel interference. Fig. 4, depicts pre-detection SINR for the 46 MHz system. We note that in higher bandwidth systems, due to shorter chip duration, inter-symbol-interference (ISI) is more severe, which leads to lower overall SINR performance. For the 46 MHz system, the average SINR decreases by 14.4, 18.2, and 21.7 dB for $P_{S/I} = 4$, 2, and 0 dB, respectively. Here, we observe 14.9, 19.8, 8.92 dB improvements in predetection SINR for the adaptive system. We note that as the interference strength reduces, the co-channel interference immunity of the static (non-optimized waveform) system improves and the performance improvement offered by adaptive channelization diminishes. Furthermore, we observe that adaptive channelization offers SINR performance improvement for a range of medium to low interferer powers.

In Fig. 5, we show experimental results from two different

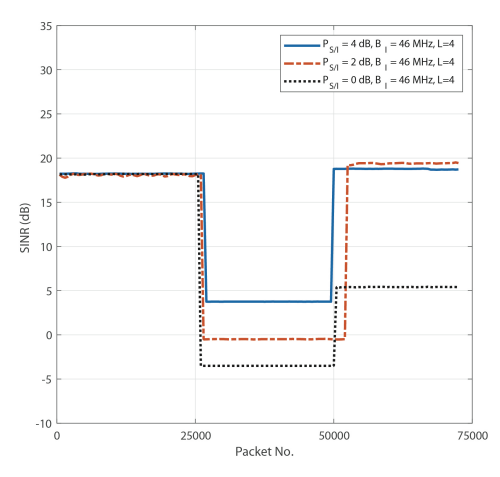


Fig. 4: Pre-detection SINR vs. packet no. in the presence of a co-channel same-band interferer ($\beta=46$ MHz).

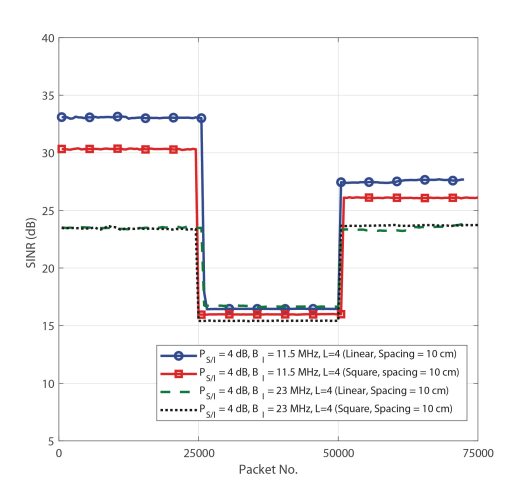


Fig. 5: Pre-detection SINR vs. packet number for two antenna formations: 1) linear and 2) square positioning with 10 cm spacing ($\beta=11.5,\ 23\ \mathrm{MHz}$).

antenna formations, specifically linear and square formation with inter-antenna spacing set to 10 cm. We plot the predetection SINR vs. packet number for an 11.5 MHz and a 23 MHz links. First, we observe that as the bandwidth of the link gets larger, the link suffers more from ISI. Specifically, the 11.5 MHz link in static (non-optimized waveform) mode operates in an SINR region of 30-35 dB, whereas the 23 MHz link operates in a 20-25 dB region. Furthermore, comparing linear and square antenna formations for the 11.5 MHz link, we observe that in static mode, the square formation performs almost 2 dB below than the linear formation (possibly due to changes in the array's propagation pattern). When the interferer is turned on $(P_{S/I} = 4 \text{ dB})$, all the links experience almost the same degradation. During operation with the spacetime optimized waveform, the linear formation produces SINR gains of 10.9 dB and the square formation about 10.07 dB. Comparing the linear and square formations for the 23 MHz link, we observe that both operate almost identically.

V. CONCLUSIONS

We designed and implemented for the first time on an RFSoC SDR interference-avoiding waveforms that are dynamically optimized in the joint space-time domain. We demonstrated significant improvements (up to 25 dB) in predetection SINR in the presence of a co-channel, same-band interferer. We also validated in practice that the proposed generalized beamforming design can be applied to transceivers with arbitrary antenna formations.

REFERENCES

- L. Chettri and R. Bera, "A comprehensive survey on internet of things (iot) toward 5g wireless systems," *IEEE Internet of Things Journal*, vol. 7, no. 1, pp. 16–32, 2019.
- [2] Y. Cao, T. Jiang, and Z. Han, "A survey of emerging m2m systems: Context, task, and objective," *IEEE Internet of Things Journal*, vol. 3, no. 6, pp. 1246–1258, 2016.
- [3] G. Sklivanitis, A. Gannon, S. N. Batalama, and D. A. Pados, "Addressing next-generation wireless challenges with commercial software-defined radio platforms," *IEEE Communications Magazine*, vol. 54, no. 1, pp. 59–67, 2016.
- [4] Q. Zhao and A. Swami, "A survey of dynamic spectrum access: Signal processing and networking perspectives," in 2007 IEEE International Conference on Acoustics, Speech and Signal Processing - ICASSP '07, vol. 4, 2007, pp. IV-1349-IV-1352.
- [5] J. Peha, "Approaches to spectrum sharing," *IEEE Communications Magazine*, vol. 43, no. 2, pp. 10–12, 2005.
- [6] I. F. Akyildiz, W.-Y. Lee, M. C. Vuran, and S. Mohanty, "A survey on spectrum management in cognitive radio networks," *IEEE Communica*tions magazine, vol. 46, no. 4, pp. 40–48, 2008.
- [7] G. Naik, J. Liu, and J.-M. J. Park, "Coexistence of wireless technologies in the 5 ghz bands: A survey of existing solutions and a roadmap for future research," *IEEE Communications Surveys & Tutorials*, vol. 20, no. 3, pp. 1777–1798, 2018.
- [8] G. Sklivanitis, E. Demirors, A. M. Gannon, S. N. Batalama, D. A. Pados, and T. Melodia, "All-spectrum cognitive channelization around narrowband and wideband primary stations," in 2015 IEEE Global Communications Conference (GLOBECOM). IEEE, 2015, pp. 1–7.
- [9] G. Sklivanitis, A. Gannon, K. Tountas, D. A. Pados, S. N. Batalama, S. Reichhart, M. Medley, N. Thawdar, U. Lee, J. D. Matyjas *et al.*, "Airborne cognitive networking: Design, development, and deployment," *IEEE Access*, vol. 6, pp. 47 217–47 239, 2018.
- [10] J. Zhang, E. Björnson, M. Matthaiou, D. W. K. Ng, H. Yang, and D. J. Love, "Prospective multiple antenna technologies for beyond 5g," *IEEE Journal on Selected Areas in Communications*, vol. 38, no. 8, pp. 1637–1660, 2020.
- [11] Y. Abdulkadir, O. Simpson, N. Nwanekezie, and Y. Sun, "Space-time opportunistic interference alignment in cognitive radio networks," in 2016 IEEE Wireless Communications and Networking Conference. IEEE, 2016, pp. 1–6.
- [12] K. Tountas, G. Sklivanitis, and D. A. Pados, "Directional space-time waveform design for interference-avoiding mimo configurations," in 2019 International Workshop on Antenna Technology (iWAT). IEEE, 2019, pp. 235–238.
- [13] Z. Liu, D. Sun, L. Liu, and K. Yi, "Joint interference suppression for multi-user tdd mimo downlink with other-cell interference," *IEEE* communications letters, vol. 16, no. 3, pp. 307–309, 2012.
- [14] R. Zhang and Y.-C. Liang, "Exploiting multi-antennas for opportunistic spectrum sharing in cognitive radio networks," *IEEE Journal of selected* topics in signal processing, vol. 2, no. 1, pp. 88–102, 2008.
- [15] R. A. Osman, S. N. Saleh, and Y. N. Saleh, "A novel interference avoidance based on a distributed deep learning model for 5g-enabled iot," *Sensors*, vol. 21, no. 19, p. 6555, 2021.
- [16] S. Naderi, D. A. Pados, G. Sklivanitis, E. S. Bentley, J. Suprenant, and M. J. Medley, "Self-optimizing near and far-field mimo transmit waveforms," *IEEE Journal on Selected areas in Communications*, 2024.
- [17] M. Golay, "Complementary series," IRE transactions on information theory, vol. 7, no. 2, pp. 82–87, 1961.
- [18] F. Ling, Synchronization in digital communication systems. Cambridge University Press, 2017.